Optimized aircraft disembarkation considering COVID-19 regulations

Schultz, M. and Soolaki, M.

This is an accepted manuscript of an article published by Taylor & Francis in Transportmetrica B: Transport Dynamics, 10 (1), pp. 880-900.

The final definitive version is available online:

https://doi.org/10.1080/21680566.2021.1965051

Preprint - Article

Optimized aircraft disembarkation considering COVID-19 regulations

Michael Schultz[1] and Majid Soolaki[2]

[1] Institute of Logistics and Aviation, Dresden University of Technology
[2] Lochlann Quinn School of Business, University College Dublin

Received: date; Accepted: date; Published: date

Abstract: Passenger disembarkation is an important handling process and takes place in the confined space of the aircraft cabin. While boarding can be controlled to a certain extent, passenger disembarkation at the end of a flight takes place in a less controllable environment. Under the current COVID 19 boundary conditions, cabin processes must not only be efficient in terms of time but also significantly reduce any potential risk of virus transmission to passengers. For this complex challenge, we have developed a novel mathematical model that takes these conflicting objective functions into account to optimize the disembarkation process. Using already enhanced seat allocations, we have developed a genetic algorithm that can generate enhanced disembarkation sequences for groups of passengers (e.g. families or couples). The selected use cases for seat loads of 50%, 66%, and 100% indicate a significant reduction in 40% disembarkation time when physical distances between passenger groups are mandatory to satisfy pandemic regulations. To inform passenger groups about the disembarkation sequences, we propose to activate the cabin lights at the seats in a dedicated way. That means that our developed methodology could already be applied to actual flights.

Keywords: passenger disembarkation, virus transmission, COVID-19, pandemic requirements, passenger groups in aircraft cabin, two-objective mathematical modeling

1. Introduction

The COVID-19 situation will have a lasting impact on air transportation in general and on both ground operations at the airport (aircraft turnaround) and passenger handling in particular. The current pandemic situation requires two major changes in the processes of the standard aircraft turnaround: (a) during aircraft disembarkation and boarding, passengers have to comply with a defined physical distance, and (b) in addition to the standard cleaning procedures the aircraft cabin has to be disinfected. The cabin disinfection before the aircraft boarding should limit possible virus transmission via surface contacts. Fig. 1 exhibits that the mandatory process changes will significantly impact the aircraft turnaround time, given that these processes are part of the critical operational path. Research that considers COVID-19 restrictions for passenger boarding [1] and aircraft cleaning [2] emphasizes the need for appropriate process adjustments to mitigate the effects of the significantly extended process times. The challenge of orderly disembarkation is still an open topic.

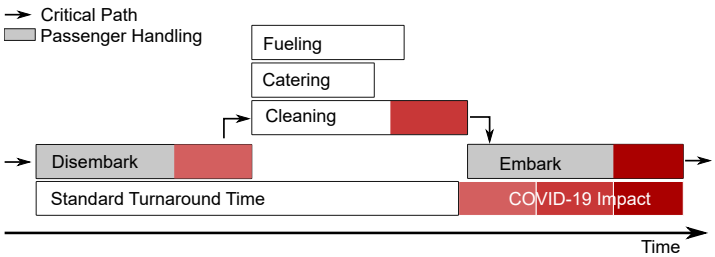

Figure 1. Impact of COVID-19 regulations on aircraft turnaround operations and time.

There are several approaches for infrastructural changes to the aircraft cabin, but most of these ideas are far away from being a flexible and standardized solution for the aviation industry. Wearing a

mask easily reduces the transmission risk during boarding and disembarkation. From the operational point of view, adapted boarding strategies are more likely to be implemented in actual airline and airport operations than altered cabin layouts. Disembarkation is more difficult to be controlled by regulations and passengers have demonstrated little discipline and high eagerness to leave the aircraft. This is particularly noteworthy because virus transmission risk during unregulated disembarkation is substantially higher than during a regulated aircraft boarding [3].

In our approach, we assume that passengers are traveling in groups and disembarkation could be controlled using the available technical infrastructure. The idea behind the consideration of group constellations is that the group members, in the sense of families or couples, were already in close contact before boarding the aircraft and should not be subject to the regulations on maintaining physical distances. We propose to use the seat-based lighting system in the aircraft cabin to allow groups of passengers to get up and leave the aircraft. Besides, the passengers themselves will initially be responsible for maintaining the minimum distance rule to other groups, with the cabin crew monitoring this process. In a follow-up stage, this process will be supported by new technologies, which can provide precise passenger locations and allow automated monitoring and controlling of passenger movements via personal devices (see Fig. 2).

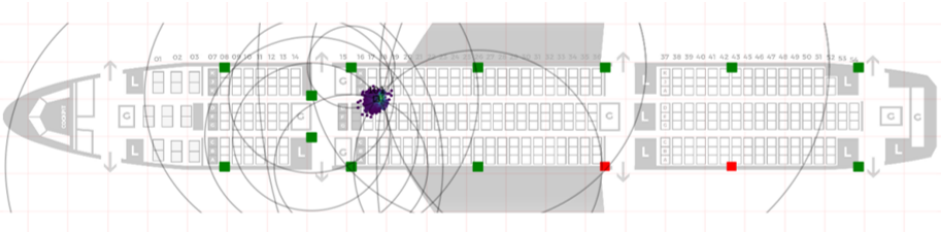

Figure 2. Estimation of passenger position based on localization framework in a digital connected cabin using stationary anchors (red and green circles) and signals from mobile devices [4].

Aircraft cabins naturally have demanding conditions for wireless signals due to possible reflections, scattering, and attenuation of the transmitted signals. In this context, the Ultra-Wide Band (UWB) technology will allow precise real-time localization for indoor application and could provide reliable distance measurements to comply with COVID-19 regulations [4]. UWB is already built into personal devices for the customer market. In the context of future aircraft operations, an efficient sensor environment will be a key element to manage passenger activities in the aircraft cabin by providing an advanced situational awareness about individual positions and system states (e.g. occupation of the aisle or status of overhead compartments). This information could be used to further improve operational efficiency and will enable new product developments and passenger-oriented services.

1.1. Review of state of the art

Comprehensive overviews are provided for passenger boarding research [5–7] and aircraft ground operations [8]. Only a few aircraft boarding and disembarkation tests have been conducted to provide data for the calibration of input parameters and validation of simulation results: using a mock Boeing 757 fuselage [9], time to store hand luggage items in the overhead compartments [10], small-scale laboratory tests [11], evaluation of passenger perceptions during boarding and disembarkation [12], operational data and passenger data from field trial measurements [13], field trials for real-time seat allocation in connected aircraft cabin [14], and using a B737-800 mock-up (1/3 size) to explore the factors affecting the time of luggage storage [15]. Although these field data are used for simulation experiments, they only cover regular behavior in a pre-pandemic situation.

The particular movement behavior of pedestrians depends significantly on group constellations (e.g. friends or families) and impacts the self-organization capabilities of crowds [16–18]. Also in the context of passenger dynamics in the airport, it is an important fact that up to 70% of the tourists and

30% of the business passengers are traveling in groups [19]. Thus, group constellations are important to understand granular flow patterns during boarding and disembarkation (e.g. couples or families are not separated). Group behavior may shorten the processes time since conflicts during the seating process are internally solved [20] and aircraft boarding by rows should be a recommended practice [10]. An approach of a dynamically optimized boarding indicates that the boarding process benefits from the consideration of groups [21]. Furthermore, less complex boarding strategies (e.g. random or block boarding) benefit more from the consideration of passenger groups (approx. 5% faster boarding), while seat-based strategies (separation of the window, middle, and aisle seats) lead to longer boarding times [5].

While passenger boarding research exhibits a broad range of improvements (e.g. group boarding, sequence optimization, infrastructural changes), research in the specific field of passenger disembarkation is quite limited and findings often arise as a side product. Two general concepts are addressed to analyze the efficacy of block-wise (aggregated seat rows) or column-wise (e.g. all aisle seats) strategies. Here, column-wise disembarkation was found to be more effective for narrow-body aircraft [22]. These two structured disembarkation strategies are analyzed in small scale field trials applying inside-out (column-wise) and back-to-front (block-wise) strategies [23], but in contrast to the prior simulation experiment [24], no significant improvements of the disembarkation time could be demonstrated.

Currently, the research focus is set on efficient passenger handling in the aircraft cabin during pandemic situations. Standard boarding strategies are analyzed considering the quantity and quality of passenger interactions and evaluated with a virus transmission model to provide a more detailed assessment. The implementation of physical distances indicates that conventional boarding strategies take longer and trade-offs between economic efficiency (seat load) and process duration must be made to minimize the impact on various health risks [25]. Adjusted seat allocation strategies are developed considering both distances to the aisle (ensure lower transmission risks caused by aisle movements) and distance between the occupied seats [26]. Furthermore, investigation shows that physical distances between passengers decrease the number of possible transmissions by approx. 75% for random boarding sequences, and could further decreased by more strict reduction of hand luggage items (less time for storage, compartment space is always available) [3]. Furthermore, standard process times could be reached if the rear aircraft door is used for boarding and disembarkation. This investigation also points out that disembarkation consists of the highest transmission potential and only minor benefits from distance rules and hand luggage regulations. The optimized consideration of passenger groups in the context of a pandemic boarding scenario will significantly contribute to a faster process (reduction of time by about 60%) and a reduced transmission risk (reduced by 85%), which reaches the level of boarding times in pre-pandemic scenarios [1]. The results of the passenger process evaluation considering the current COVID-19 situation were taken as input to further investigate the impact of pandemic requirements on the aircraft turnaround [2]. Here an integrated cleaning and disinfection procedure was developed and optimized. Under COVID-19 constraints, aircraft turnarounds require between 10% (with additional personnel) and 20% (without additional personnel) more ground time. Finally, in the context of aircraft handling, aircraft disembarkation has not yet been properly addressed and is missing to complete the picture of COVID-19's operational impacts [27].

1.2. Focus and structure of document

We provide in our contribution an approach for aircraft disembarkation considering a physical distance between groups of passengers (e.g. families or couples). In previously conducted research, we have already shown that the consideration of passenger groups shortens boarding time while maintaining the distance requirements from the COVID-19 regulations. Assuming that passengers do not get up from their seats until they are requested to do so, we develop a mathematical model to determine an improved disembarkation sequence.

The paper is structured as follows. After the introduction (Sec. 1), we briefly introduce a stochastic cellular automaton approach, which is used for modeling the passenger movements in the aircraft cabin (Sec. 2). A transmission model is implemented to evaluate the virus transmission risk during passenger movements is proposed additionally. In Sec. 3, we motivate and introduce a problem description to derive optimized sequences of passenger groups during disembarkation. Our approach allows weighting disembarkation time and a transmission risk indicator in the objective function. The results of the optimization model are presented in Sec. 4, where we use a genetic algorithm for solving the complex problem of disembarkation by providing an optimized sequence of passenger groups. This sequence is then implemented in the cellular automaton model to verify the results. Finally, we conclude our research with a summary and an outlook (Sec. 5).

2. Model for passenger disembarkation

The individual movement behavior of passengers in the aircraft cabin is modeled by a cellular automaton approach [5], which covers short (e.g. avoid collisions, group behavior) and long-range interactions (e.g. tactical wayfinding). This cellular automaton model is based on an individual transition matrix, which contains the transition probabilities to move to adjacent positions around the current position of the passenger [28].

2.1. Operational constraints and rules of movement

The implemented cellular automaton model considers operational conditions of aircraft and airlines (e.g. seat load factor, conformance to the boarding procedure) as well as the non-deterministic nature of the underlying passenger processes (e.g. hand luggage storage) and was calibrated with data from the field [13]. The cellular automaton for aircraft disembarkation is based on a regular grid (Fig. 3), which consists of equal cells with a size of 0.4 x 0.4 m, whereas a cell can either be empty or contain exactly one passenger. In the simulation, passengers can only move by one cell per time step or are required to stop if the cell in the direction of movement is occupied. To allow comparability with preliminary studies, the maximum passenger speed for disembarkation is set to 0.8 m/s, similar to boarding. This speed correlates to a time step size of 0.5 s. It may be noticed, that the speed of passengers in the aisle during disembarkation was measured to be 0.99 m/s (20% faster) [13], which also means that the finally provided disembarkation times are conservative estimations.

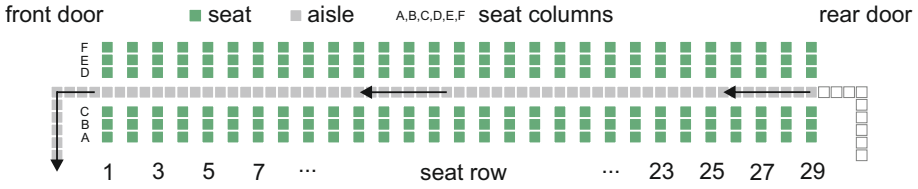

Figure 3. Grid-based aircraft model with 29 seat rows and 6 seats per row (reference layout for single-aisle, narrow-body configurations). To determine an improved sequence we assume that only the front door will be used.

The aircraft disembarkation consists of a simple set of rules for the passenger movement: (a) all passengers are seated in the aircraft according to an initial seat configuration, (b) passengers could enter the aisle if the seats at their corresponding row are free and the aisle is not blocked by other passengers, (c) if passengers enter the aisle, they take their hand luggage items out of the overhead compartment (modeled by an individual time distribution) and block this aisle cell, (d) if all hand luggage items are taken, passengers move in the direction of the assigned aircraft door by entering empty aisle cells in front of them. Further details regarding the general model and the simulation environment are available at [5].

The distribution of the time needed to pick up the hand luggage items t_p is defined by a Weibull distribution (1), with the shape parameter α and the scale parameter β.

$$F\left(t_{\mathrm{p}}, \alpha, \beta\right) = 1 - exp\left(-\frac{{t_p}^{\alpha}}{\beta}\right) \tag{1}$$

For the hand luggage storage process, the parameters are set to $\alpha = 1.7$ and $\beta = 16.0\ s$ [13]. We implemented these settings but further assume that pick up hand luggage takes half the time of the storage process, as many passengers simply take their items out of the overhead bin and make arrangements outside the cabin. Since the seat load of the cabin is reduced to comply with COVID-19 regulations, the utilization of the overhead bins is also at a low level. Thus an additional consideration of an occupancy index for the bins is not needed [29].

In each simulation step, the list of passengers to be updated is randomly shuffled to emulate a parallel update behavior for the discrete time dynamics (random-sequential update) [28,30]. Passengers in the aisle move forward to the next cell, if possible (free aisle cell and hand luggage were already taken out of the overhead compartment). Passengers in the seat rows enter the aisle when adjacent seats are free and the corresponding aisle cell is not blocked. For the COVID-19 scenarios, a cell is assumed to be blocked if entering the aisle or moving in the aisle would infringe the separation distance between the passenger (groups).

Depending on the seat load given, passengers or passenger groups are randomly allocated in the aircraft. Each disembarkation scenario is simulated 125,000 times, to achieve statistically relevant results defined by the average boarding time. The disembarkation starts when the first passenger enters the aisle and finishes when the last passenger leaves the aircraft. In contrast to the aircraft boarding, we assume 100% compliant behavior of passengers in following the proposed disembarkation sequence. During boarding, late arrivals or priority rules impact the initial sequence of passengers and result often in extended process times [31,32].

In the context of physical distance, the International Aviation Transport Association (IATA) demands a distance of at least 1 meter [33] and the Federal Aviation Administration (FAA) a minimum of 6 feet (2 meters) [34]. Considering the cellular automaton model with a grid structure of 0.4 x .4 m cells, and to maintain comparability of our results with preliminary studies [1–3], the minimum physical distance was set to 1.6 m (4 cells). At this point, we assume that passengers are informed that a distance of 1.6 m corresponds to the distance of 2 seat rows, which offers proper visual guidance.

2.2. Transmission model

The fundamental cellular automaton developed for the stochastic passenger movements is extended by an approach to evaluate the risk of virus transmission during the boarding process. The transmission risk can be defined by two major input factors: distance to the index case and reduction of contact time. A straightforward approach is to count both the individual interactions (passengers located in adjacent cells) and the duration of these contacts in the aisle and during the seating process. However, counting the individual contacts will only provide the first indication about potential ways of infections [3]. Our implemented approach based on a transmission model [35] defining the spread of the coronavirus SARS-CoV2 as a function of different public distancing measures [36]. Herein, the probability of a person n to become infected by person m is described according to (2).

$$P_n = 1 - exp\left(-\theta \sum_{m} \sum_{t} \mathrm{SR}_{m,t} \quad i_{nm,t} \quad t_{nm,t}\right) \tag{2}$$

defined by:

- P_n the probability of the person n to receive an infectious dose. This shall not be understood as "infection probability", because this strongly depends on the immune response by the affected person.
- θ the calibration factor for the specific disease.
- $\mathrm{SR}_{m,t}$ the shedding rate, the amount of virus the person m spreads during the time step t.

$i_{nm,t}$ the intensity of the contact between n and m during the time step t, which corresponds to their distance.

$t_{nm,t}$ the time the person n interacts with person m during the time step t.

Considering this idea, we define the shedding rate SR as a normalized bell-shaped function (3) with $z \in (x, y)$ for both longitudinal and lateral dimensions, respectively. The parameters are a (scaling factor), b (slope of leading and falling edge), and c (offset) to determine the shape of the curve.

$$\mathrm{SR}_{xy} = \prod_{z \in (x,y)} \left(1 + \frac{|z - c_z|^{2b_z}}{a_z} \right)^{-1} \tag{3}$$

In a preceding study [3], SR was calibrated on the transmission events of an actual flight [37]. Thus, we are using the corresponding parameter setting with $a_x = 0.6$, $b_x = 2.5$, $c_x = 0.25$, $a_y = 0.65$, $b_y = 2.7$, and $c_y = 0$. This generates a slightly smaller footprint in y-direction (lateral to moving direction) than in x-direction (longitudinal to moving direction). Additionally, the spread in x-direction is higher in front of the index case than behind it. Consequently, the moving direction is changed by 90 degrees with a heading to the aircraft window, when the passenger arrives his seat row.

Finally, the individual probability for virus transmission P_n is corresponds to Θ, the specific intensity (dose) per time step (4).

$$P_n = \Theta \ \mathrm{SR}_{xy} \ \alpha \tag{4}$$

In accordance with [3], Θ is set to $\frac{1}{20}$, which means a passenger reaches a probability of $P_n = 1$ after standing 20 s in closest distance in front of an infected passenger ($\mathrm{SR}_{xy} = 1$). The parameter $\alpha \in \{1, 2\}$ is 1 and changed to 2 when the passenger stores the luggage or enters the seat row. This doubled shedding rate reflects the higher physical activities within a short distance to surrounding passengers.

3. Optimized disembarkation of passenger groups

A new analytical approach for the passenger boarding problem during the COVID-19 situation was developed, which introduces passenger groups and appropriate seat allocation patterns [1]. We continue this research and similarly assume that an airline decides to assign only a percentage of the available seats to reduce the virus transmission probability in the cabin. Therefore, we use the already defined use cases for the 50%, 66%, and 100% seat load of an Airbus A320 cabin (29 seat rows, 174 seats).

Further, group members are considered as a community (e.g. a family) and the transmission probability is only relevant between members of different groups. An appropriate seat allocation provides a space between groups and groups with a large number of members should be seated in the rear of the aircraft [1]. In Fig. 4 an example is given for 50% case to show how 31 passenger groups of different sizes are allocated in the aircraft cabin accordingly. Here, the passengers are separated into eight single travelers (green), nine groups consist of two passengers (blue), five groups with three members (purple), three groups of four and five passengers (pink and red), two groups of six passengers (orange) and a group of seven passengers (yellow).

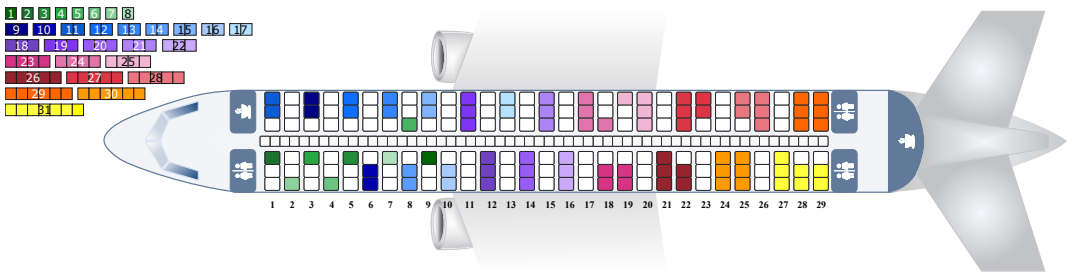

Figure 4. Optimized seat allocation of 31 passengers groups considering spaces around groups [1].

Also, in our prior research, we generated the optimized boarding plans for 66 and 100 percentages including 166 and 174 passengers respectively [1]. The number of groups is increased to generated those scenarios. For example, in the last scenario, they considered 62 groups. As our focus is on the disembarkation process regarding the COVID-19 situation, therefore we use these results as the inputs of our new analytical approach. In other words, the optimized seat design plans of passengers are selected based on Fig. 5.

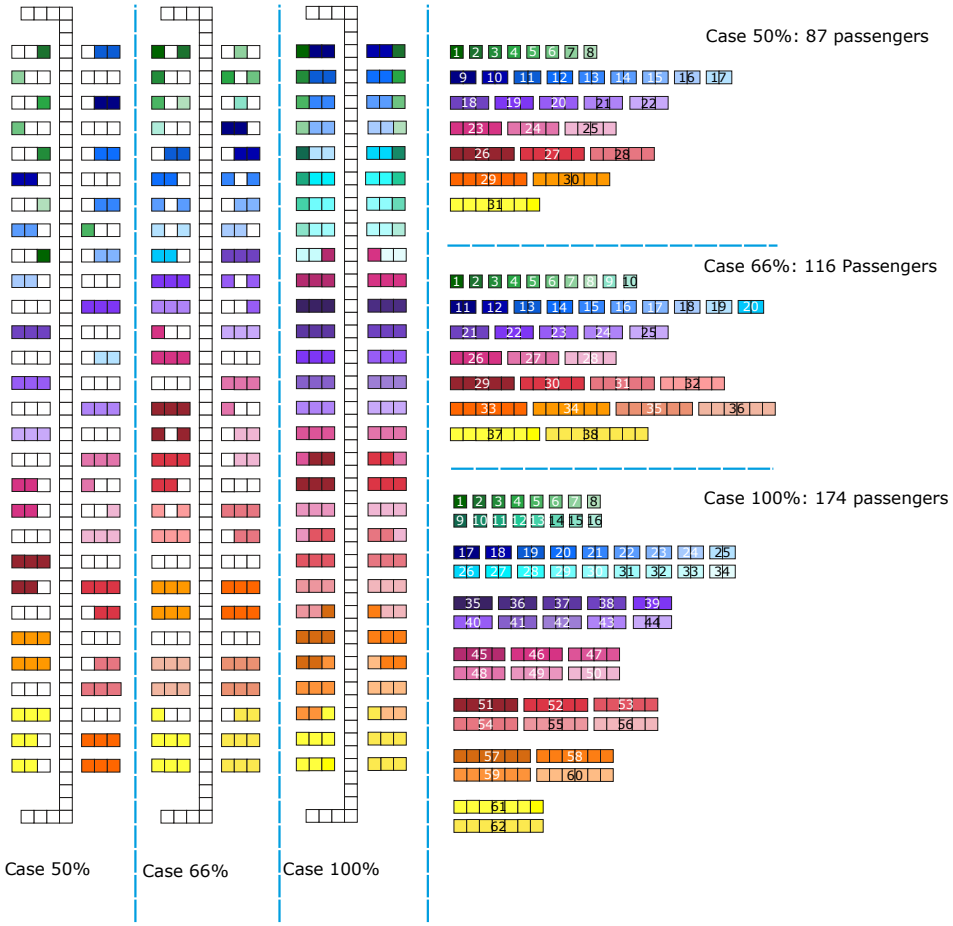

Figure 5. Three seat allocations for 50%, 66% and 100% seat load [1], which are used as application cases. A numerical representation is provided in the annex.

In a first and simplified approach, passenger groups were disembarked by batches of passenger groups. Here, groups of a batch are permitted to enter the aisle, making sure that the minimum distance between the groups is maintained at any time. After a group has received permission to disembark, the members of the group enter the aisle, take their hand luggage and wait until the group in front of them starts moving. Groups from the following batch could start when the last group of the current batch passed their seat row. This procedure ensures a minimal disembarkation time. In future operational scenarios, passenger groups may directly be informed via personal devices or active lights at their seats to start for disembarkation. Key enabling technology for this approach will be a highly reliable and precise determination of passenger locations.

A sensitivity analysis is conducted to show how the time for disembarkation changes. During the analysis, we randomly select a group of passengers from the example case above (Fig. 4 and add this group to the current disembarkation batch with a defined probability. This probability increases from 0% (one group per batch) to 100% (all groups in one batch) in 10% steps. Furthermore, three levels for hand luggage are considered: 100% - standard, 50% - reduced, 0% - no items. For the reference case, the scenario with only one group per batch (no hand luggage items) is used. The

average disembarkation times and the associated standard deviations are depicted in Fig. 6. The analysis shows that disembarkation will benefit from the superior organization of groups into batches up to a certain point. As a result, average disembarkation times decrease until a minimum is reached at approximately 80%. In general, the standard deviations exhibit also a minimum in that region (70% - 90%) but show both a significant increasing and decreasing behavior. The reason is that if all passenger groups are in one batch, the disembarkation is a front to back process, where groups in the front are leaving the aircraft first. This a somehow a much more stable process than a batch-organized prioritization but also results in higher disembarkation times.

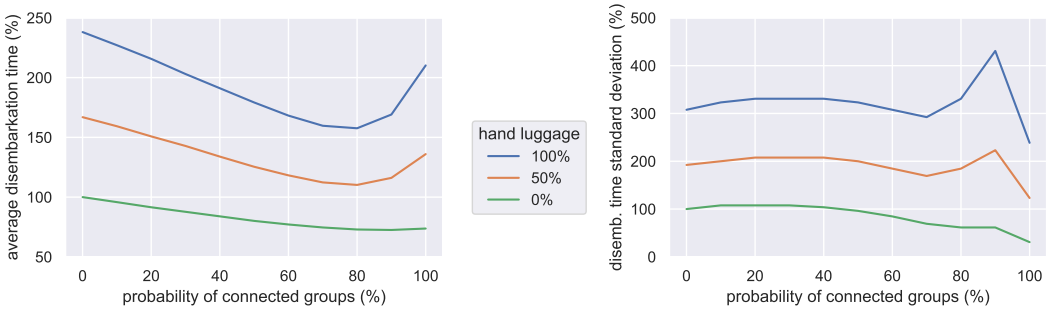

Figure 6. Random group sequence for disembarkation, assuming (a) given probability that the following group is part of the same disembarkation batch, and (b) three level of hand luggage quantity (100% - standard, 50% - reduced, 0% - no items).

The obtained minimum times indicate a significant potential to reduce the disembarkation time by about 40%. To provide a more improved disembarkation process, a manual assignment of groups will be derived from the introduced seat allocation. Each batch of passenger groups is generated starting with the last occupied seat row. The group of this row will be placed into the aisle, assuming the individual personal space (one cell per passenger). Considering the distance of 1.6 m per group, the nearest group to that location (downstream) is added to the current batch. This process is finished when the first seat row is reached. Fig. 7 exhibits this batch assignment process, where 6 batches are created for the given example. This algorithm-based batch sequence results for the three hand luggage scenarios in reduced disembarkation times by 7%, 27%, and 35% for the zero luggage, 50%, and 100% hand luggage items accordingly (referring to the corresponding minimum times presented at Fig. 6).

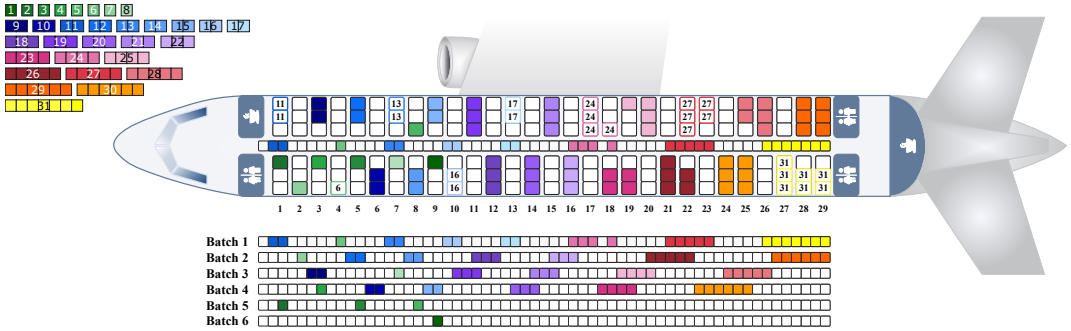

Figure 7. Batch-oriented disembarkation considering a minimum distance of 1.6 m between passenger groups. The current aisle status corresponds to the first batch. The following batches are depicted below.

These results lead to the question of how this process can be further improved. In the following section, we develop a two-objective mathematical model, which includes an optimized disembarkation strategy incorporating passenger groups and physical distance requirements from the current COVID-19 situation. In the development, we are not considering hand luggage items assuming that the average pick-up process will not influence the sequence generation.

3.1. Mathematical Problem Description and Formulation

The concept of the shedding rates was already applied for the aircraft boarding [1] and is now used for the disembarkation process. Here, the corresponding shedding rate depends on the position of the infected passenger in the aisle and the positions of the passengers of other groups that will leave their seats afterward. We calculate the transmission risk function for all passengers based on the locations of other passengers (see Fig. 8). For example, suppose that the last group (coded yellow) is walking in the aisle. We show the different types of shedding rates that we computed at this moment for the passengers of this group. For example, for the first passenger of this group, we calculate shedding rates types 4, 5, and 6 based on the locations of passengers who seat in row 20 and column D, E, and F, respectively and similarly we consider shedding rates types 1, 2, and 3 for the third passenger of this group based on the locations of passengers who seat in row 21 and column A, B, and C.

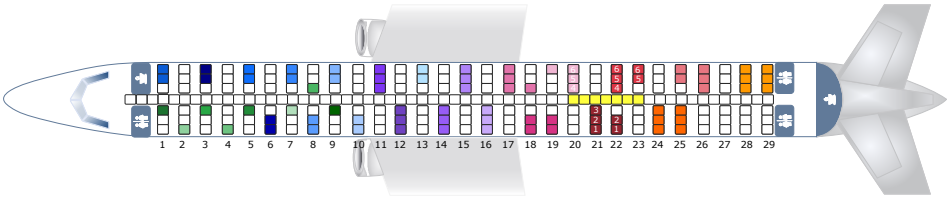

Figure 8. Spatial dependencies of the shedding rate.

As this study focuses on the disembarkation process, we consider the shedding rates for passengers when they are walking in the aisle. We defined the interference type two to handle the situation. For each group, the time needed to leave the aircraft are defined by the numbers of rows to pass (distance) and columns the members occupied (window, middle, aisle seats). For example, group 30 (light orange, six members seated in rows 24 and 25 at Fig. 8) needs more time to leave the aircraft than a group with the same number of members sitting in the front of the aircraft or a group with fewer members in the same seat row(s). We consider the parameter λ_{ij} (5) for disembarkation time for a passenger who is seated in row i and column j, using a numerical representation for the seat columns {1,...,6} for {A,...,F}.

$$\lambda_{ij} = \begin{cases} i + 4 - j & \text{if} \quad j \in \{1,2,3\} \\ i + j - 3 & \text{if} \quad j \in \{4,5,6\} \end{cases} \tag{5}$$

Taking into account the maximum speed of passengers (0.8 m/s) and the relevant aisle length of 23.2 m (29 rows with a seat pitch of 0.8 m), a passenger who seats on row 29 and column F ($j = 6$) has a disembarkation time of $29 + 6 - 3 = 32s$.

Three types of passenger interference are implemented in our approach. The first type is defined based on the concept of physical distancing. We suppose a close distance between members of each group in the aisle. As a result, if the group thirty of six members starts in the two last rows $i = 28, 29$, they will block rows numbers $i = 27$ to $i = 29$ because there is a $0.8m$ distance between seats of each row. According to the COVID-19 regulations and our group approach, an additional physical distance of 1.6 m between groups is implemented (see Fig. 9, part 1).

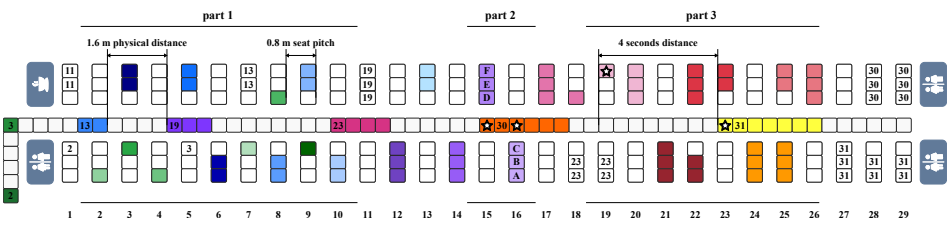

Figure 9. Different types of interference between passengers in the aisle of aircraft.

The second type of interference is defined regarding the concept of the shedding rate of infected passengers for the other passengers that are seated in the cabin. If an infected passenger leaves the seat, the several shedding rates must be counted based on the location of the other group members who will leave the aircraft after that passenger.

Taking Fig. 9 (part 2) as an example, we show the interference generated in the two middle rows ($i = 15$ and $i = 16$), when the first member of group thirty (coded orange) are walking in the aisle at period h, we compute the shedding rates for the passengers from other groups that seat in the related row ($i = 15$ at column D (aisle), E (middle), and F (window)). Similarly, the third member of this group could generate different types of interactions for passengers who seat in the next row at the same time ($i = 16$ at column C (aisle), B (middle), and A (window)).

As a result, if the passengers of the first group leave the aircraft earlier, the transmission risk which is the sum of shedding rates of all passengers could be minimized. On the other hand, this strategy leads to longer disembarkation time. Therefore, we have proposed a two-objective mathematical model to handle these two conflicting objectives. The third type of interference is the scheduling process. Taking Fig. 9 (part 3) as an example, if the first member of group number 31 arrives in the nineteenth row ($i = 19$) in four seconds then, the passenger who seated in the row $i = 19$ and column F (window) could not leave the seat at that moment. Based on these types of interference and the nature of the disembarkation problem, we present the assumptions as follows.

- The members of each group start leaving their seats at the same time.
- There is a gap of time (e.g. three time steps) to leave the seats for members of two different groups, which seated in a close zone. The gap increases with the number of group members.
- The length of the aisle in the cabin would be 23.2m.
- The transmission rates are calculated for all passengers.
- When a passenger leaves the seat and walks in the aisle, (s)he could not be blocked by another passenger during the disembarkation period.

3.2. Optimization Model

The sets, parameters, decision variables, and multi-objective model are developed in this section.

Notation	**Definition**
Sets and Indexes	
i	Index set of row $i \in \{1, 2, \ldots, \mathcal{I}\}$
k	Index set of passenger group $k \in \{1, 2, \ldots, \mathcal{K}\}$
j	Index set of seat column $j \in \{1, 2, \ldots, \mathcal{J}\}$
h	Index set of time period $h \in \{1, 2, \ldots, \mathcal{H}\}$
r	Index set of interaction type $r \in \{1, 2, \ldots, \mathcal{R}\}$
Parameters	
T_k	Number of group number k
$SR_j^{'}$	The related shedding rate for interaction j or r because we consider six different types based on the number of columns
λ_{ij}	The disembarkation time (in period unit) required for a passenger who seats in a seat in row i and column j
Y_{ij}	Binary parameter, equals k if a passenger from group k is seated in a seat in row i and column j; equals zero otherwise
$M_{kk'}$	Binary parameter, equals one if the members of groups number k and k' could not leave their seats at the same time (because they will block each other such as groups numbers 30 and 31), equals zero otherwise
w_1	the coefficient weight of the first objective function $w_1 \in [0, 1]$
w_2	the coefficient weight of the second objective function which is equals to $1 - w_1$
Decision Variables	
p_{kh}	The number of members of group k that leave their seats at time period h
x_{ijkh}	Binary variable, equals one if a passenger from group k who is seated in a seat in row i and column j leaves its seat at the time period h (activation time); equals zero otherwise
q_{ijkh}	The period of time from the moment when a passenger from group k in row i and column j leaves the cabin
$n_{iji'}$	The period of time at the moment when a passenger who has seated in row i and column j reaches to the row i'
$u_{kk'hh'}$	Binary variable, equals one if group k and k' leave their seats at time period h and h', respectively
z_1	First objective function: disembarkation time
z_2	Second objective function: Transmission Risk Indicator
TZ	Total objective function which is calculated based on two conflicted objectives z

The proposed new multi-objective minimization model for the problem is introduced as follows.

$$TZ = w_1\left(\frac{z_1 - {z_1}^*}{{z_1}^*}\right) + w_2\left(\frac{z_2 - {z_2}^*}{{z_2}^*}\right) \tag{6}$$

$$\text{Disembarkation Time:} \quad z_1 = \underset{i\in\mathcal{I},j\in\mathcal{J},k\in\mathcal{K},h\in\mathcal{H}}{Max} \quad q_{ijkh} \tag{7}$$

$$\text{Transmission Risk Indicator:} \quad z_2 = \sum_{i=1}^{\mathcal{I}}\sum_{j=1}^{\mathcal{J}}\sum_{\substack{k=1\\k=Y_{ij}}}^{\mathcal{K}}\sum_{h=1}^{\mathcal{H}}\sum_{i'=i}^{\mathcal{I}}\sum_{j'=1}^{\mathcal{J}}\sum_{k'=Y_{i'j'}}^{\mathcal{K}}\sum_{h'=1\ h'<h-n_{i'j'i}}^{\mathcal{H}} SR_j^{'}u_{kk'hh'} \tag{8}$$

$$\sum_{i=1}^{\mathcal{I}}\sum_{j=1}^{\mathcal{J}}\left(\frac{x_{ijkh}}{T_k}\right) + \sum_{i=1}^{\mathcal{I}}\sum_{j=1}^{\mathcal{J}}\sum_{h'=h}^{h+T_k+3}\left(\frac{x_{ijk'h'}}{T_{k'}}\right) \le 1 \qquad \forall h,k,k', M_{kk'}=1 \tag{9}$$

$$0.4\sum_{i=1}^{\mathcal{I}}\sum_{j=1}^{\mathcal{J}}\sum_{k=1}^{\mathcal{K}}\sum_{\substack{h'=1\\h'>h-\lambda_{ij}}}^{h} x_{ijkh'} + 1.6\sum_{i'=1}^{\mathcal{I}}\sum_{j'=1}^{\mathcal{J}}\sum_{k'=1}^{\mathcal{K}}\sum_{\substack{h'=1\\h'>h-\lambda_{i'j'}}}^{h}\left(\frac{x_{i'j'k'h'}}{T_{k'}}\right) \le 23.2 \qquad \forall h>1 \tag{10}$$

$$\sum_{i=1}^{\mathcal{I}}\sum_{j=1}^{\mathcal{J}} x_{ijkh} = p_{kh} \qquad \forall k,h \tag{11}$$

$$\sum_{h=1}^{\mathcal{H}} x_{ijkh} = 1 \qquad \forall i,j,k=Y_{ij} \tag{12}$$

$$T_k x_{ijkh} \le \sum_{i'=1}^{\mathcal{I}}\sum_{j'=1}^{\mathcal{J}} x_{i'j'kh} \qquad \forall i,j,k,h \tag{13}$$

$$p_{kh} + p_{k'h'} - 1 \le u_{kk'hh'} \qquad \forall k,k',h,h' \tag{14}$$

$$q_{ijkh} \ge h + \lambda_{ij} + 500(x_{ijkh} - 1) \qquad \forall i,j,k,h \tag{15}$$

$$q_{ijkh} \le 500 x_{ijkh} \qquad \forall i,j,k,h \tag{16}$$

$$n_{iji'} = \lambda_{ij} - i' + h \qquad \forall i,j,k=Y_{ij},h,x_{ijkh}=1 \tag{17}$$

$$x_{i'j'k'h'} \le |h' - n_{iji'}| \qquad \forall i,i',j,j',h',k=Y_{ij},k'=Y_{i'j'},k\neq k'>0 \tag{18}$$

$$x_{ijkh}, u_{kk'hh'} \in \{0,1\}, \quad q_{ijkh}, n_{iji'}, p_{kh}, z_1, z_2 \ge 0 \qquad \forall i,i',j,k,k',h,h' \tag{19}$$

The $L-1$ metric method is used to solving the multi-objective decision problem. Therefore, we run the model three times. In the first time, we minimize the average disembarkation time of all passengers by equation (7) as objective function subject to constraints (9)-(18). Therefore, the first ideal solution z_1^* could be obtained here. Similarly, we minimize the problem regarding the second objective function which is the sum of shedding rates as transmission risk indicator by equation (8) and under constraints (9)-(18). Therefore, we obtain the second ideal solution z_2^* and implement these two ideal solutions in the general problem at the last step. In the other words, we minimize equation (6) as an objective function subject to constraints (7)-(18). Here, we consider two implement weights (i.e. w_1 and w_2) for conflicting objectives which assess and determine by decision-makers.

Constraints (9) guarantee that at each time step, two groups that are seated in a close zone, could not leave their seats at the same time. The physical distances between passengers in the aisle are corresponded by constraints (10). Here, we calculate the distances between members of each group and between two different groups as well. In each time step, we consider $0.4m$ between the members

of the same group in the aisle and $1.6m$ as a physical distance between the last member of a group and the first passenger of the next group in the aisle. Constraints (11) compute the number of members of each group that leave their seats at each period. Also, constraints (12)-(13) guarantee that all members of each group leave their seats at the same period. To calculate the decision variables for the shedding rates of two different groups, we define constraints (14) which are implemented in the transmission risk function. Constraints (15)-(16) represent the disembarkation time of each passenger in each group that seated in row i and column j, and corresponding decision variable takes zero if the seat was not occupied. The third type of interference are formulated in constraints (17)-(18). In the other words, for each passenger, we compute the time (i.e. $n_{iji'}$) that (s)he arrives at the lower row i' by constraints (17), and as a result, we do not allow to passengers of that row to leave their seats at that time by constraints (18). Finally, constraints (19) represent the requirements for decision variables.

4. Application of the model and evaluation of the results

The proposed new mathematical model as a scheduling problem is a type of NP-hard and as a result, the optimization solvers could not find an optimal solution in a reasonable time. For the validation of the model, we created a small size problem including six rows and columns including five groups in sixty periods of time. Then we solved it with the optimization software GAMS, but when we increased the size of the problem, the software could not find an optimal solution in a limitation of 12 hours. For the real size of the problem, we consider 29 rows, 6 columns, 3 interaction types, 31 groups, and 500 periods of time (or seconds). We exemplarily implement the optimized seat allocation as depicted in Fig. 4. To solve the problem we implement a meta-heuristic algorithm. Therefore, a Genetic Algorithm (GA) is designed to solve the real size problem. A laptop with the specifications of AMD Ryzen 7, 3700U, 2.30GHz CPU, 16 GB RAM, and Matlab 2020 software is used for running the code of GA.

4.1. Solution procedure and results

We suggested using a GA to solve the disembarkation problem because it has a great application in solving combinatorial optimization problems. Also, some researchers designed GA as a effective solution approach for seat layout/boarding/disembarkation problem [38,39]. Here, we represent the proposed chromosome structure as follows:

$$C = \left[c_{i,j,k}\right]_{\mathcal{I}\times\mathcal{J}\times\mathcal{K}}, \quad \text{if} \quad y_{i,j} = k \quad \text{and} \quad x_{i,j,k,h} = 1, \quad \text{then} \quad c_{i,j,k} \quad \text{takes} \quad h, \quad \text{otherwise zero.}$$

If the seat (row i, column j) was assigned to a passenger of group k, and the passenger leaves the seat at time h, therefore the decision variable $x_{i,j,k,h}$ takes one, and as a result, the value of the array of the matrix C (i.e. $c_{i,j,k}$) takes h. For example, if the passengers of group thirty ($k = 30$) leave their seats at time $h = 150s$ then, we use the sub matrix below:

$$C_{29\times6\times30} = \begin{bmatrix} 0 & 0 & 0 & 0 & 0 & 0 \\ 0 & 0 & 0 & 0 & 0 & 0 \\ \dots & \dots & \dots & \dots & \dots & \dots \\ 0 & 0 & 0 & 0 & 0 & 0 \\ 0 & 0 & 0 & 150 & 150 & 150 \\ 0 & 0 & 0 & 150 & 150 & 150 \end{bmatrix}$$

As the first generation, we create the population of chromosomes under the structure of matrix C. To calculate the fitness function value of each chromosome, we use the value of the original objective function plus the three penalties if the constraints (9), (10), and (18) are violated. To create the next generations of chromosomes, we implement the selection, mutation, crossover, elitism, and migration operators.

The roulette wheel is used as our selection operator. Regarding the roulette wheel, the chromosomes with lower fitness function values have a higher chance of selection. We use the crossover operator to create new children of two selected parents. First of all, the numbers of groups are randomly divided in two sets (i.e. S^1 and S^2). As an example, for the groups numbers 30 and 31 if we suppose that $30 \in S^1$ and $31 \in S^2$ and the following arrays:

$$C^{Parent1} = \left[c_{i,j,k}\right]_{\mathcal{I}\times\mathcal{J}\times\mathcal{K}} \qquad C^{Parent2} = \left[c_{i,j,k}\right]_{\mathcal{I}\times\mathcal{J}\times\mathcal{K}}$$

$$C_{29\times6\times30}^{Parent\ 1} = \begin{bmatrix} 0 & 0 & 0 & 0 & 0 & 0 \\ 0 & 0 & 0 & 0 & 0 & 0 \\ \cdots & \cdots & \cdots & \cdots & \cdots & \cdots \\ 0 & 0 & 0 & 0 & 0 & 0 \\ 0 & 0 & 0 & 150 & 150 & 150 \\ 0 & 0 & 0 & 150 & 150 & 150 \end{bmatrix} \quad C_{29\times6\times31}^{Parent\ 1} = \begin{bmatrix} 0 & 0 & 0 & 0 & 0 & 0 \\ 0 & 0 & 0 & 0 & 0 & 0 \\ \cdots & \cdots & \cdots & \cdots & \cdots & \cdots \\ 100 & 100 & 100 & 0 & 0 & 0 \\ 100 & 100 & 0 & 0 & 0 & 0 \\ 100 & 100 & 0 & 0 & 0 & 0 \end{bmatrix}$$

$$C_{29\times6\times30}^{Parent\ 2} = \begin{bmatrix} 0 & 0 & 0 & 0 & 0 & 0 \\ 0 & 0 & 0 & 0 & 0 & 0 \\ \cdots & \cdots & \cdots & \cdots & \cdots & \cdots \\ 0 & 0 & 0 & 0 & 0 & 0 \\ 0 & 0 & 0 & 80 & 80 & 80 \\ 0 & 0 & 0 & 80 & 80 & 80 \end{bmatrix} \quad C_{29\times6\times31}^{Parent\ 2} = \begin{bmatrix} 0 & 0 & 0 & 0 & 0 & 0 \\ 0 & 0 & 0 & 0 & 0 & 0 \\ \cdots & \cdots & \cdots & \cdots & \cdots & \cdots \\ 180 & 180 & 180 & 0 & 0 & 0 \\ 180 & 180 & 0 & 0 & 0 & 0 \\ 180 & 180 & 0 & 0 & 0 & 0 \end{bmatrix}$$

Then the first child receives their genes or the arrays in Matrix C from the first parent which are related to the first set (S^1) and the other genes from the second parent. In a similar way, the second child receives their genes of first sets (S^1) from the second parents and the others from the first parent. The result is presented here:

$$C_{29\times6\times30}^{Child\ 1} = \begin{bmatrix} 0 & 0 & 0 & 0 & 0 & 0 \\ 0 & 0 & 0 & 0 & 0 & 0 \\ \cdots & \cdots & \cdots & \cdots & \cdots & \cdots \\ 0 & 0 & 0 & 0 & 0 & 0 \\ 0 & 0 & 0 & 150 & 150 & 150 \\ 0 & 0 & 0 & 150 & 150 & 150 \end{bmatrix} \quad C_{29\times6\times31}^{Child\ 1} = \begin{bmatrix} 0 & 0 & 0 & 0 & 0 & 0 \\ 0 & 0 & 0 & 0 & 0 & 0 \\ \cdots & \cdots & \cdots & \cdots & \cdots & \cdots \\ 180 & 180 & 180 & 0 & 0 & 0 \\ 180 & 180 & 0 & 0 & 0 & 0 \\ 180 & 180 & 0 & 0 & 0 & 0 \end{bmatrix}$$

$$C_{29\times6\times30}^{Child\ 2} = \begin{bmatrix} 0 & 0 & 0 & 0 & 0 & 0 \\ 0 & 0 & 0 & 0 & 0 & 0 \\ \cdots & \cdots & \cdots & \cdots & \cdots & \cdots \\ 0 & 0 & 0 & 0 & 0 & 0 \\ 0 & 0 & 0 & 80 & 80 & 80 \\ 0 & 0 & 0 & 80 & 80 & 80 \end{bmatrix} \quad C_{29\times6\times31}^{Child\ 2} = \begin{bmatrix} 0 & 0 & 0 & 0 & 0 & 0 \\ 0 & 0 & 0 & 0 & 0 & 0 \\ \cdots & \cdots & \cdots & \cdots & \cdots & \cdots \\ 100 & 100 & 100 & 0 & 0 & 0 \\ 100 & 100 & 0 & 0 & 0 & 0 \\ 100 & 100 & 0 & 0 & 0 & 0 \end{bmatrix}$$

The diversity of solutions is maintained by the mutation operators in the designed GA. Therefore, some genes in a selected chromosome are changed in each population/generation and then, new chromosomes will be created for the next generation. Here, we implement three mutation operators. In the first mutation operator, we generate a random group for a selected chromosome and then we change the positive genes randomly which means we update the disembarkation time for that group. In the second mutation operator, we select two random groups, and then the positive arrays of two groups are changed which means the disembarkation times of that two groups are changed. In the last mutation operator, if for all groups, we do not have a disembarkation time for a specific time, we reduce that time. As a result, for the groups with disembarkation times that are larger than that

specific time, we subtract one unit of their disembarkation times. We transfer a low percentage of a generation to the next generation by migration operator. Finally, the high-quality chromosomes in terms of fitness function value are transferred to the next generation by the elitism operator. In the designed GA, we use the setting below for executing the GA code: number of initial population = 200, generations = 400, crossover rate = 0.5, mutation rate = 0.3, migration rate = 0.05 and elitism = 0.15.

4.2. Results of the analytical model and designed GA

We consider the optimized seat layouts that are generated by Schultz and Soolaki [1] as the inputs of the designed GA (see Fig. 5). Therefore, the Fig. 5 depicts the optimized seat layouts of thirty-one, thirty-eight and sixty-two groups. Also, we consider ten minutes ($h = 600s$) as an upper bound of disembarkation for all passengers. To calculate the second type of interference (see Fig. 9) between passengers in the aisle, we use the equation (3) based on the distance between the infected passenger in the aisle and the other passengers who seat at that moment.

As mentioned previously, we have developed a new two objectives mathematical modeling. The first objective function indicates the disembarkation time of all passengers and the second objective targets the transmission risk indicator. In the following, we provide the solutions for four exemplary scenarios (see Fig. 10 - 13, a numerical representation is provided in the annex).

1. **Scenario A1** - Minimizing disembarkation time, 50% seat load
   Here we minimize the first objective function for 87 passengers. The coefficient weight of disembarkation time equals one and the coefficient weight of the transmission risk indicator supposes zero. The optimized disembarkation plan for this scenario is indicated in Fig. 10. The disembarkation time for the first scenario is 139 s and the transmission risk indicator from the second objective function is calculated in the value of 480. In Fig. 10 the proposed sequence is shown and the locations of all passengers in the aisle are indicated in the 0.5 s time steps.

2. **Scenario A2** - Minimizing transmission risk indicator, 50% seat load
   In this scenario, the second objective function for 87 passengers is minimized. The coefficient weight of disembarkation time equals zero and the coefficient weight of the transmission risk is supposed to be one. To compare with the first scenario, although the value of transmission risk decreases from 480 to 30, the disembarkation time increases by 50%. The reason behind this comes from when we are disembarkation the passengers in the same rows or in the near zone, it takes more time to leave their seats. For example, the gap time between groups number 30 (orange color in row 28 and 29) and 31 (yellow color in row 27, 28, and 29) is considered about 9 s (see Fig. 11). Also, our focus is on the disembarkation time, and therefore, we just define one scenario (scenario A2) to compare the first two scenarios in terms of the fitness functions. Therefore, in the third and last scenarios, we just minimize the first objective functions.

3. **Scenario B** - Minimizing disembarkation time, 66% seat load
   The number of passengers is selected to 116 and we consider 38 different groups. In this scenario, we minimize the disembarkation time. In other words, the coefficient of the first objective function is supposed to be 1. Fig 12 indicates the output plan for this scenario. As we can see, the value of disembarkation time is 188 s.

4. **Scenario C** - Minimizing disembarkation time, 100% seat load
   In the last scenario, we suppose the cabin is fully occupied. The number of passengers is 174 and we consider 62 different groups. As Fig. 13 indicates the optimized plan and it takes 299 s to leave all of the passengers from the cabin.

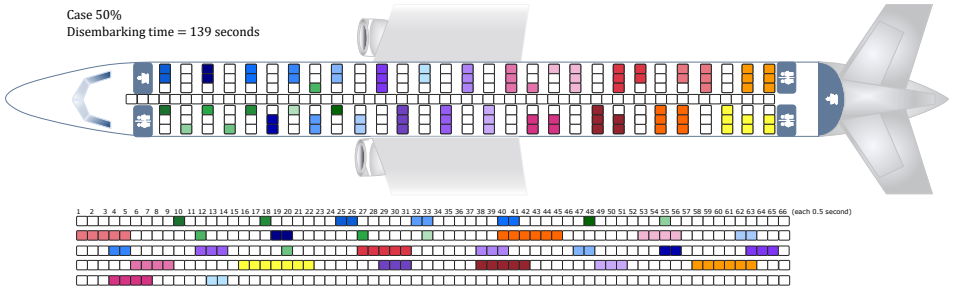

Figure 10. The proposed disembarkation plan for scenario A1 (87 passengers)

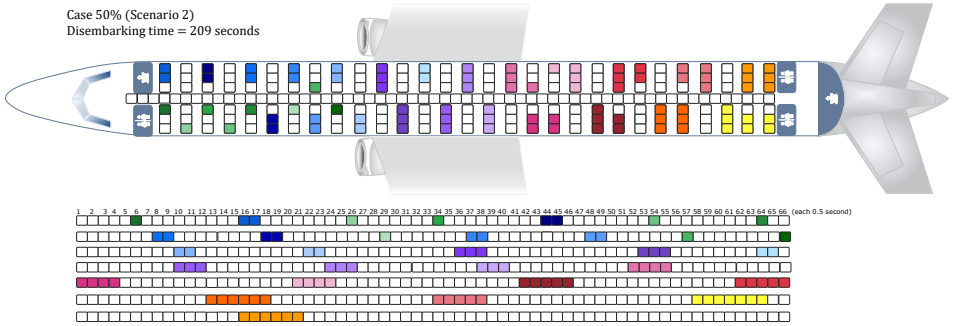

Figure 11. The proposed disembarkation plan for scenario A2 (87 passengers)

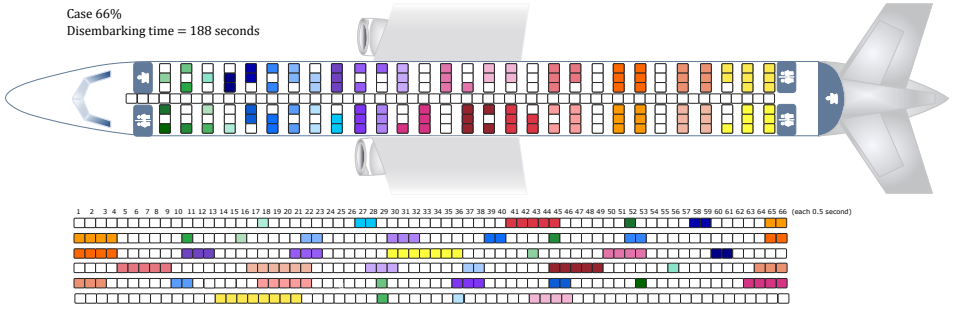

Figure 12. The proposed disembarkation plan for scenario B (116 passengers)

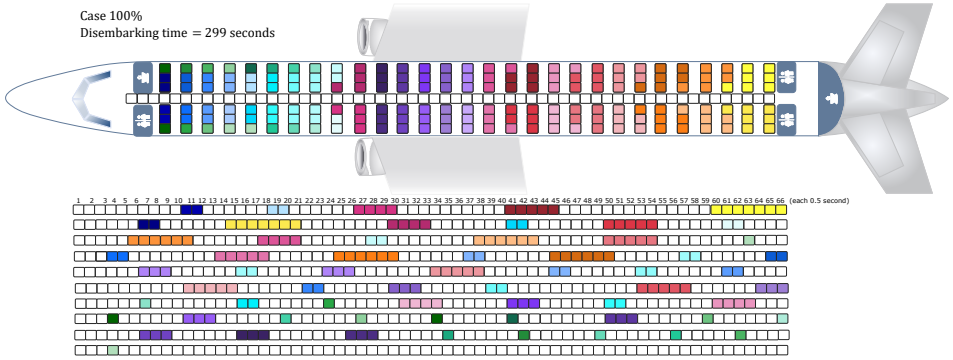

Figure 13. The proposed disembarkation plan for scenario C (174 passengers)

4.3. Evaluation of disembarkation process

At this stage, we have to emphasize again that our current approach to find appropriate sequences is not considering different times for the individual pick up of hand luggage items. We assume that every passenger will immediately leave the cabin after entering the aisle. So the pickup process would only increase the disembarkation time, but on average does not affect the order of the groups. As shown in the exemplary presented solutions (Fig. 10-13), we assume a forward ordered-sequential update of passenger passenger positions [40]. Thus, the update of the positions starts with the passenger closest to the exit (front door) and the positions of the subsequently following passengers along the aisle will be updated next during one time step. The consequences of this approach are that groups always use the narrowest space in the cabin and the disembarkation time is calculated optimistically.

With this in mind, we implemented the optimized group sequences in the calibrated stochastic simulation environment to verify the results of the disembarkation time. In this environment, every group is activated to disembark when the group that is directly in front of them in the disembarkation sequence passes their seat row. This minimizes the possible buffers between group calls as would be necessary for later operational implementation. The group members do not enter the aisle until the physical distance between the groups is ensured. Tab. 1 summarizes the simulation results. The result from the forward ordered-sequential update implementation underestimates the disembarkation times by about 30 s, which is caused by the movement interactions of the passengers in the aisle. To exhibit the potential to improve the disembarkation time, we use reference cases for each scenario. These reference cases consider the same amount of passengers, no groups, no hand luggage items, physical distance, and the realistic random-sequential update behavior. Concerning the reference cases, our optimization strategy (focusing on a fast disembarkation process) accelerated the process by about 40%.

			disembarkation time (s)			
			sequential update behavior			disembarkation
scenario	seat load (%)	passengers	forward ordered	random	reference	improvement (%)
A1	50	87	139	163	286	43
B	66	116	188	219	377	42
C	100	174	299	331	571	42

Table 1. Disembarkation of passenger groups considering three scenarios with a seat load of 50%, 66%, and 100%.

5. Discussion and outlook

Along the passenger journey, the processes in the aircraft cabin require sharing a confined environment with other passengers during boarding, flight, disembarkation. These processes have the risk of virus transmission between passengers and require risk mitigation strategies. A physical distance between passenger groups during disembarkation reduces the transmission risks and an appropriate sequence for these passenger groups will contribute to a significant reduction of the disembarkation time.

We consider passenger groups as an important factor for operational efficiency. The main idea behind our approach is that members of a group should be allowed to be close to each other, as they were before joining. Different groups, however, should be as far apart as necessary. We assume that the passenger groups can be informed when they are allowed to start disembarkation. For this information process, the cabin light environment could be used today, but in a future digital connected cabin, passengers could be informed directly via their personal devices. Further, these devices could also be used to ensure appropriate distances between passengers [4].

The implementation of the optimized group sequence exhibits a potential to increase the disembarkation efficiency by a time reduction of approx. 40%. As we are aiming for an appropriate sequence, at this stage, we do not consider hand luggage items. In future research work, we will also

consider the distribution of hand luggage in the cabin and the associated times. In addition, Pareto Fronts can be defined based on the different weights of objective functions. Finally, we will investigate the potential of technological systems that can monitor, evaluate, and, if necessary, control passenger boarding and disembarkation.

6. Appendix

In this appendix, the detailed information for the scenarios A1, B, and C are provided using a numerical description of the seat allocation and activation times.

Scenario A1 - seat allocation (group)

	A	B	C	D	E	F
1			2		11	11
2	7					
3			4		9	9
4	6					
5			3		12	12
6	10	10				
7			8		13	13
8	14	14		5		
9			1		15	15
10	16	16				
11				19	19	19
12	18	18	18			
13					17	17
14	20	20	20			
15				21	21	21
16	22	22	22			
17				24	24	24
18	23	23		24		
19	23	23				25
20				25	25	25
21	26	26	26			
22	26	26		27	27	27
23					27	27
24	29	29	29			
25	29	29	29		28	28
26				28	28	28
27	31	31	31			
28	31	31		30	30	30
29	31	31		30	30	30

Scenario A1 - activation times (s)

	A	B	C	D	E	F
1			0		5	4
2	18					
3			33		33	32
4	64					
5			0		5	5
6	80	80				
7			29		54	53
8	1	1		25		
9			5		73	73
10	47	47				
11				74	74	74
12	93	94	94			
13					117	117
14	48	48	48			
15				65	65	65
16	95	99	99			
17				74	74	74
18	107	107		74		
19	106	106				34
20				34	34	34
21	82	83	83			
22	81	82		54	54	54
23					54	54
24	26	26	26			
25	26	26	26		6	6
26				6	6	6
27	74	74	74			
28	74	74		95	95	95
29	74	74		95	95	95

Scenario B - seat allocation (group)

	A	B	C	D	E	F
1	1		2		7	
2	3			4		6
3	5		8		9	
4	10			11	11	
5		13	13		12	12
6	14	14		15		15
7	16		16		17	17
8	19		19	18	18	
9	20	20		21	21	21
10	22	22	22	23		23
11	24	24	24			23
12	26			25	25	25
13	26	26	26			
14				27	27	27
15	29	29	29	27		
16	29		29		28	28
17	30	30	30		28	28
18	30	30				
19	32		32	31	31	31
20	32	32	32		31	31
21						
22	34	34	34	33	33	33
23	34	34	34	33	33	33
24						
25	36	36	36	35	35	35
26	36	36	36	35	35	35
27	37				38	38
28	37	37	37	38	38	38
29	37	37	37	38	38	38

Scenario B - activation times (s)

	A	B	C	D	E	F
1	149		19		79	
2	47			30		137
3	170		29		117	
4	0			84	84	
5		142	142		14	14
6	39	40		44		40
7	123		124		25	24
8	165		166	103	102	
9	0	0		56	56	55
10	129	129	130	56		55
11	19	19	19			54
12	143			95	95	94
13	143	143	143			
14				66	65	65
15	96	96	96	65		
16	96		96		158	157
17	0	0	0		157	156
18	0	0				
19	117		117	79	79	79
20	117	117	117		79	79
21						
22	1	1	1	40	40	40
23	1	1	1	40	40	40
24						
25	79	79	79	103	103	103
26	79	79	79	103	103	103
27	48				143	143
28	48	48	48	143	143	143
29	48	48	48	143	143	143

Scenario C - seat allocation (group)

	A	B	C	D	E	F
1	1	17	17	18	18	2
2	3	19	19	20	20	4
3	5	21	21	22	22	6
4	7	23	23	24	24	8
5	9	25	25	26	26	10
6	11	27	27	28	28	12
7	13	29	29	30	30	14
8	15	31	31	32	32	16
9	33	33	45	46	34	34
10	45	45	45	46	46	46
11	35	35	35	36	36	36
12	37	37	37	38	38	38
13	39	39	39	40	40	40
14	41	41	41	42	42	42
15	43	43	43	44	44	44
16	47	47	47	48	48	48
17	47	51	51	52	52	48
18	51	51	51	52	52	52
19	49	49	49	50	50	50
20	49	53	53	54	54	50
21	53	53	53	54	54	54
22	55	55	55	56	56	56
23	55	55	57	58	56	56
24	57	57	57	58	58	58
25	57	57	59	60	58	58
26	59	59	59	60	60	60
27	59	59	61	62	60	60
28	61	61	61	62	62	62
29	61	61	61	62	62	62

Scenario C - activation times (s)

	A	B	C	D	E	F
1	240	0	0		30	29	225
2	199	92	92		123	123	275
3	250	153	153		167	167	284
4	285	144	144		108	108	234
5	85	40	41		0	0	241
6	277	212	212		192	191	267
7	275	141	141		168	168	226
8	245	113	113		124	124	185
9	42	46	0		30	64	64
10	0	0	0		30	30	30
11	252	252	259		252	251	251
12	241	241	243		241	241	241
13	213	213	213		202	201	201
14	176	176	177		157	156	156
15	124	124	124		114	114	114
16	85	85	85		54	53	53
17	85	31	31		0	0	52
18	31	31	31		0	0	0
19	192	192	192		202	202	202
20	192	65	65		168	168	202
21	65	65	65		168	168	168
22	145	145	145		124	124	124
23	145	145	85		93	124	124
24	85	85	85		93	93	93
25	85	85	54		41	93	93
26	54	54	54		41	41	41
27	54	54	5		0	41	41
28	3	3	4		0	0	0
29	1	1	3		0	0	0

Table 2. Numerical representation of passenger groups seated in the aircraft cabin and the corresponding activation times for a fast disembarkation.

Conflicts of Interest: The authors declare no conflict of interest.

References

1. Schultz, M.; Soolaki, M. Analytical approach to solve the problem of aircraft passenger boarding during the coronavirus pandemic. *Transportation Research Part C: Emerging Technologies* **2021**, *124*, 102931. doi:10.1016/j.trc.2020.102931.
2. Schultz, M.; Evler, J.; Asadi, E.; Preis, H.; Fricke, H.; Wu, C.L. Future aircraft turnaround operations considering post-pandemic requirements. *Journal of Air Transport Management* **2020**, *89*, 101886. doi:10.1016/j.jairtraman.2020.101886.
3. Schultz, M.; Fuchte, J. Evaluation of Aircraft Boarding Scenarios Considering Reduced Transmissions Risks. *Sustainability* **2020**, *12*, 5329. doi:10.3390/su12135329.
4. Schwarzbach, P.; Engelbrecht, J.; Michler, A.; Schultz, M.; Michler, O. Evaluation of Technology-Supported Distance Measuring to Ensure Safe Aircraft Boarding during COVID-19 Pandemic. *Sustainability* **2020**, *12*, 8724. doi:10.3390/su12208724.
5. Schultz, M. Implementation and application of a stochastic aircraft boarding model. *Transportation Research Part C: Emerging Technologies* **2018**, *90*, 334–349. doi:10.1016/j.trc.2018.03.016.
6. Delcea, C.; Cotfas, L.A.; Paun, R. Agent-Based Evaluation of the Airplane Boarding Strategies' Efficiency and Sustainability. *Sustainability* **2018**, *10*, 1879. doi:10.3390/su10061879.
7. Jaehn, F.; Neumann, S. Airplane boarding. *European Journal of Operational Research* **2015**, *244*, 339–359. doi:10.1016/j.ejor.2014.12.008.
8. Schmidt, M. A review of aircraft turnaround operations and simulations. *Progress in Aerospace Sciences* **2017**, *92*, 25–38. doi:10.1016/j.paerosci.2017.05.002.
9. Steffen, J.H.; Hotchkiss, J. Experimental test of airplane boarding methods. *Journal of Air Transport Management* **2012**, *18*, 64–67. doi:10.1016/j.jairtraman.2011.10.003.
10. Kierzkowski, A.; Kisiel, T. The Human Factor in the Passenger Boarding Process at the Airport. *Procedia Engineering* **2017**, *187*, 348–355. doi:10.1016/j.proeng.2017.04.385.

11. Gwynne, S.M.V.; Senarath Yapa, U.; Codrington, L.; Thomas, J.R.; Jennings, S.; Thompson, A.J.L.; Grewal, A. Small-scale trials on passenger microbehaviours during aircraft boarding and deplaning procedures. *Journal of Air Transport Management* **2018**, *67*, 115–133. doi:10.1016/j.jairtraman.2017.11.008.
12. Miura, A.; Nishinari, K. A passenger distribution analysis model for the perceived time of airplane boarding/deboarding, utilizing an ex-Gaussian distribution. *Journal of Air Transport Management* **2017**, *59*, 44–49. doi:10.1016/j.jairtraman.2016.11.010.
13. Schultz, M. Field Trial Measurements to Validate a Stochastic Aircraft Boarding Model. *Aerospace* **2018**. doi:10.3390/aerospace5010027.
14. Schultz, M. Fast Aircraft Turnaround Enabled by Reliable Passenger Boarding. *Aerospace* **2018**, *5*, 8. doi:10.3390/aerospace5010008.
15. Ren, X.; Zhou, X.; Xu, X. A new model of luggage storage time while boarding an airplane: An experimental test. *Journal of Air Transport Management* **2020**, *84*, 101761. doi:10.1016/j.jairtraman.2019.101761.
16. Moussaïd, M.; Perozo, N.; Garnier, S.; Helbing, D.; Theraulaz, G. The Walking Behaviour of Pedestrian Social Groups and Its Impact on Crowd Dynamics. *PLOS ONE* **2010**, *5*, 1–7. doi:10.1371/journal.pone.0010047.
17. Schultz, M.; Rößger, L.; Fricke, H.; Schlag, B. Group Dynamic Behavior and Psychometric Profiles as Substantial Driver for Pedestrian Dynamics. In *Pedestrian and Evacuation Dynamics 2012*; Springer International Publishing, 2013; pp. 1097–1111. doi:10.1007/978-3-319-02447-9_90.
18. Zanlungo, F.; Yücel, Z.; Kanda, T. Intrinsic group behaviour II: On the dependence of triad spatial dynamics on social and personal features; and on the effect of social interaction on small group dynamics. *PLOS ONE* **2019**, *14*, 1–28. doi:10.1371/journal.pone.0225704.
19. Schultz, M.; Fricke, H. Managing Passenger Handling at Airport Terminal. 9th USA/Europe Air Traffic Management Research and Development Seminar; , 2011.
20. Tang, T.Q.; Yang, S.P.; Ou, H.; Chen, L.; Huang, H.J. An aircraft boarding model accounting for group behavior. *Journal of Air Transport Management* **2018**, *69*, 182–189. doi:10.1016/j.jairtraman.2018.03.004.
21. Zeineddine, H. A dynamically optimized aircraft boarding strategy. *Journal of Air Transport Management* **2017**, *58*, 144–151. doi:10.1016/j.jairtraman.2016.10.010.
22. Wald, A.; Harmon, M.; Klabjan, D. Structured deplaning via simulation and optimization. *Journal of Air Transport Management* **2014**, *36*, 101–109. doi:10.1016/j.jairtraman.2014.01.001.
23. Qiang, S.; Jia, B.; Huang, Q. Evaluation of Airplane Boarding/Deboarding Strategies: A Surrogate Experimental Test. *Symmetry* **2017**, *9*, 222. doi:10.3390/sym9100222.
24. Qiang, S.J.; Jia, B.; Jiang, R.; Huang, Q.X.; Radwan, E.; Gao, Z.Y.; Wang, Y.Q. Symmetrical design of strategy-pairs for enplaning and deplaning an airplane. *Journal of Air Transport Management* **2016**, *54*, 52–60. doi:10.1016/j.jairtraman.2016.03.020.
25. Cotfas, L.A.; Delcea, C.; Milne, R.J.; Salari, M. Evaluating Classical Airplane Boarding Methods Considering COVID-19 Flying Restrictions. *Symmetry* **2020**, *12*, 1087. doi:10.3390/sym12071087.
26. Salari, M.; Milne, R.J.; Delcea, C.; Kattan, L.; Cotfas, L.A. Social distancing in airplane seat assignments. *Journal of Air Transport Management* **2020**, *89*, 101915. doi:10.1016/j.jairtraman.2020.101915.
27. Xie, C.Z.; Tang, T.Q.; Hu, P.C.; Huang, H.J. A civil aircraft passenger deplaning model considering patients with severe acute airborne disease. *Journal of Transportation Safety & Security* **2021**, *0*, 1–22. doi:10.1080/19439962.2021.1873879.
28. Schultz, M. Stochastic Transition Model for Pedestrian Dynamics. In *Pedestrian and Evacuation Dynamics 2012*; Springer International Publishing, 2013; pp. 971–985. doi:10.1007/978-3-319-02447-9_81.
29. Ren, X.; Zhou, X.; Xu, X. A new model of luggage storage time while boarding an airplane: An experimental test. *Journal of Air Transport Management* **2020**, *84*, 101761. doi:10.1016/j.jairtraman.2019.101761.
30. Schultz, M. Entwicklung eines individuenbasierten Modells zur Abbildung des Bewegungsverhaltens von Passagieren im Flughafenterminal. PhD thesis, Technische Universität Dresden, Faculty of Transport and Traffic Sciences "Friedrich List", Dresden, 2010.
31. Schultz, M. Implementation and application of a stochastic aircraft boarding model. *Transportation Research Part C: Emerging Technologies* **2018**, *90*, 334–349. doi:10.1016/j.trc.2018.03.016.
32. Zeineddine, H. Reducing the effect of passengers' non-compliance with aircraft boarding rules. *Journal of Air Transport Management* **2021**, *92*, 102041. doi:10.1016/j.jairtraman.2021.102041.

33. International Aviation Transport Association (IATA). Guidance for Cabin Operations During and Post Pandemic, edt. 4, 2020.
34. Federal Aviation Administration (FAA). COVID-19: Updated Interim Occupational Health and Safety Guidance for Air Carriers and Crews, 2020.
35. Smieszek, T. A mechanistic model of infection: why duration and intensity of contacts should be included in models of disease spread. *Theor Biol Med Model* **2009**, *6*. doi:https://doi.org/10.1186/1742-4682-6-25.
36. Müller, S.A.; Balmer, M.; Neumann, A.; Nagel, K. Mobility traces and spreading of COVID-19. *medRxiv* **2020**. doi:10.1101/2020.03.27.20045302.
37. Olsen, S.J.; Chang, H.L.; Cheung, T.Y.Y.; Tang, A.F.Y.; Fisk, T.L.; Ooi, S.P.L.; Kuo, H.W.; Jiang, D.D.S.; Chen, K.T.; Lando, J.; Hsu, K.H.; Chen, T.J.; Dowell, S.F. Transmission of the Severe Acute Respiratory Syndrome on Aircraft. *New England Journal of Medicine* **2003**, *349*, 2416–2422. doi:10.1056/NEJMoa031349.
38. van den Briel, M.H.L.; Villalobos, J.R.; Hogg, G.L.; Lindemann, T.; Mulé, A.V. America West Airlines Develops Efficient Boarding Strategies. *INFORMS Journal on Applied Analytics* **2005**, *35*, 191–201. Publisher: INFORMS.
39. Soolaki, M.; Mahdavi, I.; Mahdavi-Amiri, N.; Hassanzadeh, R.; Aghajani, A. A new linear programming approach and genetic algorithm for solving airline boarding problem. *Applied Mathematical Modelling* **2012**, *36*, 4060–4072. doi:10.1016/j.apm.2011.11.030.
40. Schadschneider, A.; Chowdhury, D.; Nishinari, K. Chapter Two - Methods for the Description of Stochastic Models. In *Stochastic Transport in Complex Systems*; Schadschneider, A.; Chowdhury, D.; Nishinari, K., Eds.; Elsevier: Amsterdam, 2011; pp. 27–70. doi:10.1016/B978-0-444-52853-7.00002-6.